tween the Cp ligands and the two guanosine residues as well as between the Cp ligands and the phosphate backbone (Figure 18). The modeling studies show that Cp_2Mo^{2+}-nucleobase bidentate coordination to mutually tipped guanosine residues such as those in *cis*-$[Pt(NH_3)_2\{d(pGpG)\}]$[7a,d] is also sterically impaired. These observations are in agreement with results to be reported elsewhere[67] which indicate that the binding of $Cp_2VCl_2(aq)$ or $Cp_2MoCl_2(aq)$ to DNA plasmids and the subsequent effects on DNA processing enzymes are greatly different from those of cisplatin.[4,7] While NMR data provide no evidence for strong $Cp_2MoCl_2(aq)$ binding to various ribose/nucleobase-terminated model oligonucleotides, binding is observed to 5'-phosphate terminated oligonucleotides.[67] Thus, it is likely that the mechanism(s) of Cp_2MX_2 antineoplastic activity is (are) quite different from that (those) of cisplatin. It if furthermore conceivable that mechanisms are different for different metallocene drugs, and these possibilities are presently under investigation.

(67) (a) Liu, A. H.; Kuo, L. Y.; Marks, T. J., manuscript in preparation. (b) Liu, A. H.; Marks, T. J., manuscript in preparation.

Acknowledgment. This research was supported by NSF (Grant CHE8800813). L.Y.K. was a Dee and Moody Predoctoral Fellow. We thank Dr. W. C. Finch for assistance with the solid-state ^{31}P NMR spectroscopy and Dr. A. H. Liu for assistance with the molecular graphics.

Supplementary Material Available: Tables of atomic coordinates (Tables III, IV, and IX) and anisotropic thermal parameters for **3a**, **4**, and **5**, hydrogen atom positions for **3a** and **4**, and $^1H-^1H$ coupling constants and derived conformational populations for **5**, **6**, and **7a** (10 pages); listings of observed and calculated structure factors from the final cycles of least-squares refinement for **3a**, **4**, and **5** (78 pages). Ordering information is given on any current masthead page.

Ab Initio Prediction of the Structures and Stabilities of the Hyperaluminum Molecules: Al_3O and Square-Planar Al_4O

Alexander I. Boldyrev[†] and Paul von R. Schleyer*

Contribution from the Institut für Organische Chemie, Friedrich-Alexander Universität Erlangen-Nürnberg, Henkestrasse 42, D-8520 Erlangen, Germany. *Received February 4, 1991*

Abstract: The concept of hypermetalation, characterized by molecules with unprecedented stoichiometries, is extended to the aluminum–oxygen combinations, Al_3O and Al_4O. Their equilibrium geometries and fundamental frequencies, as well as those of the isolated reference species AlO, Al_2, Al_2^+, Al_2O, Al_3O^+, Al_3O, Al_3^+, Al_4^{2+}, and Al_4O, were calculated at HF/6-31G* and at various correlated levels, e.g., MP2(full)/6-31G*. Extensive searches of possible structures and electronic states were carried out. The global minima are: linear Al_2O ($D_{\infty h}$, $^1\Sigma_g^+$), planar Al_3O^+ (D_{3h}, $^1A_1'$), planar Al_3O (the C_{2v} $Y(^2A_1)$ and $T(^2B_2)$ forms have nearly the same energy), tetrahedral Al_4^{2+} (T_d, $^1A_1$), and planar Al_4O (D_{4h}, $^1A_{1g}$). All these species are very stable (with the exception of Al_4^{2+}) with regard to all possible decomposition pathways. Representative dissociation energies (in kcal/mol at PMP4SDTQ/6-311+G*//MP2(full)/6-31G*+ZPE) are: Al_3O^+, into $Al_2O + Al^+$ (34.1); Al_3O, into Al_2O + Al (19.9); Al_4O, into Al_3O + Al (45.5) or into $Al_2O + Al_2$ (37.1). Although the aluminum–oxygen attraction is largely ionic, aluminum–aluminum bonding contributes significantly to the stability of the hyperaluminum Al_3O and Al_4O molecules.

Introduction

We have discovered a remarkable molecule, Al_4O, computationally. The oxygen is surrounded by four aluminum atoms in a square-planar (D_{4h}) arrangement. The electronic structure, combining ionic and substantial metal–metal bonding, anticipates a large, new class of similar molecules.

Such "hypermetalation" involving alkali metal stoichiometries exceeding normal valence expectations is now well-documented. Many of hyperlithium molecules (OLi_4, OLi_5, OLi_6, NLi_5, CLi_5, CLi_6, BLi_5, $BeLi_4$, $BeLi_6$, Cs_4O, etc.) were discovered computationally.[1-11] Li_3O, Li_4O, and Li_5O have been observed mass spectrometrically and the atomization energies determined.[12,13] There is similar evidence for Na_2Cl,[14] Na_3O, Na_4O, K_3O, K_4O,[15,16] and Cs_8O.[17] The "suboxides" of rubidium and cesium, e.g., Rb_9O_2, Cs_7O, and $Cs_{11}O_3$, have been characterized.[18,19] The substantial stability of these molecules is due to the high degree of ionic character as well as bonding interactions between the ligand atoms.[1-7] In a sense, hypermetalated species can be regarded as metal clusters bound ionically to a centrally located "impurity" heteroatom. This contrasts with the usual situation in which the only bonding interactions are between the central atom and its attached atoms or ligands, e.g., in methane, where the ligand–ligand interactions are repulsive. Hence, the usual valence theory, which does not include all the possible interatomic interactions as bonding possibilities, must be modified.

[†] Permanent address: Institute of Chemical Physics, USSR Academy of Sciences, Moscow V-334, Kosygin str. 4, USSR.

(1) Schleyer, P. v. R.; Wurthwein, E.-U.; Pople, J. A. *J. Am. Chem. Soc.* **1982**, *104*, 5839.
(2) Schleyer, P. v. R. *New Horizons of Quantum Chemistry*; Lowdin, P.-O., Pulman, A., Eds.; Reidel: Dordrecht, 1983; pp 95-105.
(3) Schleyer, P. v. R.; Wurthwein, E.-U.; Kaufmann, E.; Clark, T. *J. Am. Chem. Soc.* **1983**, *105*, 5930.
(4) Schleyer, P. v. R.; Tidor, B.; Jemmis, E. D.; Chandrasekhar, J.; Wurthwein, E.-U.; Kos, A. J.; Luke, B. T.; Pople, J. A. *J. Am. Chem. Soc.* **1983**, *105*, 484.
(5) Schleyer, P. v. R. *Pure Appl. Chem.* **1984**, *56*, 151.
(6) Schleyer, P. v. R.; Reed, A. E. *J. Am. Chem. Soc.* **1988**, *110*, 4453.
(7) Reed, A. E.; Schleyer, P. v. R.; Janoschek, R. *J. Am. Chem. Soc.* **1991**, *113*, 1885.
(8) Pewestorf, W.; Bonacic-Koutecky, V.; Koutecky, J. *J. Chem. Phys.* **1988**, *89*, 5794.
(9) Fantucci, P.; Bonacic-Koutecky, V.; Pewestorf, W.; Koutecky, J. *J. Chem. Phys.* **1989**, *91*, 4229.
(10) Klimenko, N. M.; Musaev, D. G.; Gorbik, A. A.; Zyubin, A. S.; Charkin, O. P.; Wurthwein, E.-U.; Schleyer, P. v. R. *Koord. Khim.* **1986**, *12*, 601.
(11) Savin, A.; Preuss, H.; Stoll, H. *Rev. Roum. Chim.* **1987**, *32*, 1069.
(12) Wu, C. H. *J. Chem. Phys.* **1976**, *65*, 3181.
(13) Wu, C. H. *Chem. Phys. Lett.* **1987**, *139*, 357.
(14) Peterson, K. I.; Dao, P. D.; Castleman, A. W., Jr. *J. Chem. Phys.* **1983**, *79*, 777.
(15) Dao, P. D.; Peterson, K. I.; Castleman, A. W., Jr. *J. Chem. Phys.* **1984**, *80*, 563.

0002-7863/91/1513-9045$02.50/0

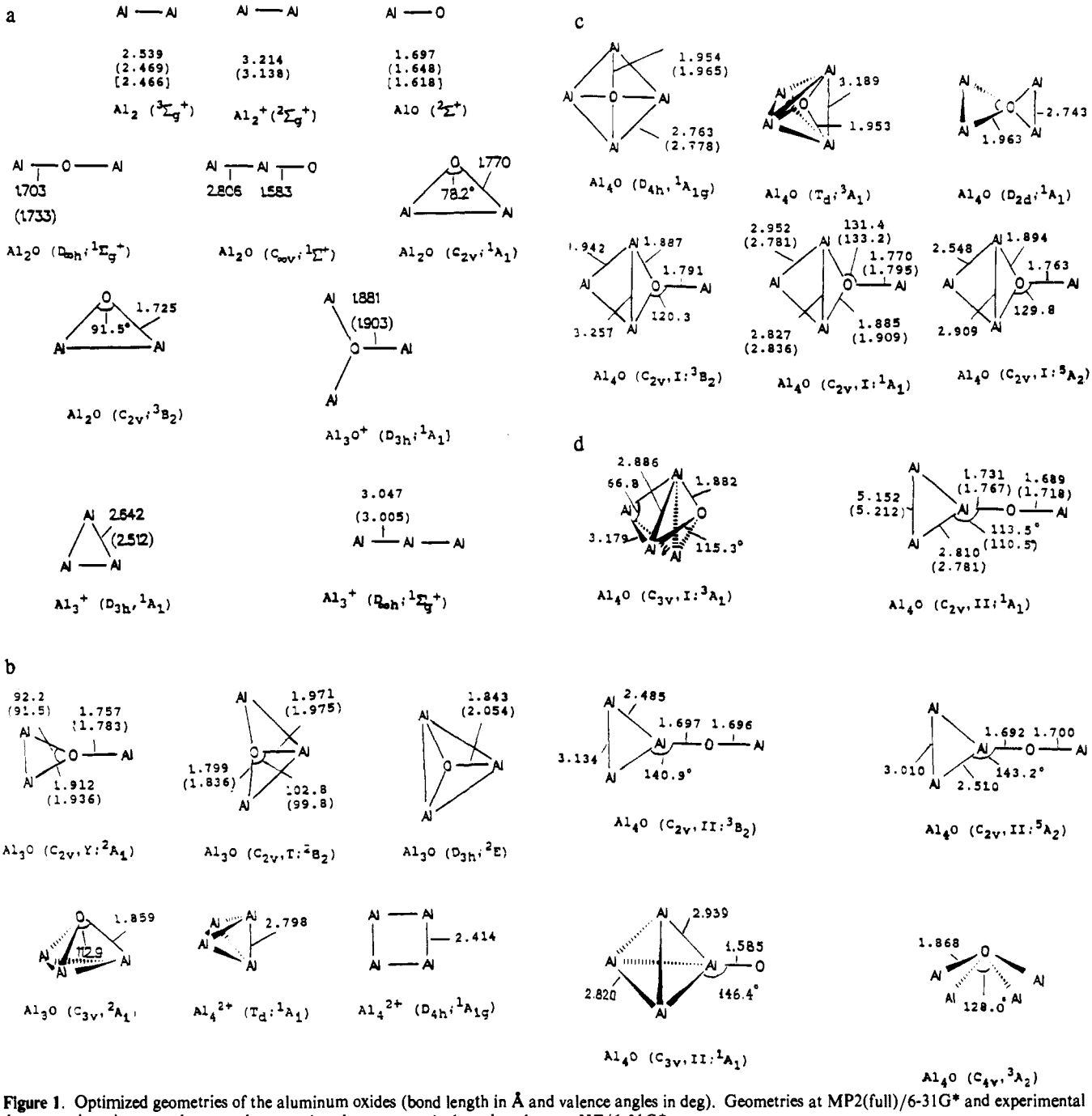

Figure 1. Optimized geometries of the aluminum oxides (bond length in Å and valence angles in deg). Geometries at MP2(full)/6-31G* and experimental data are given in parentheses and square brackets, respectively; other data at HF/6-31G*.

Although having the usual "valence", $SiLi_4$ also provides an instructive illustration. Metal–metal bonding contributes to the surprising preference for a nontetrahedral, C_{2v} point group geometry.[6,7]

Hypermetalation should be a general phenomenon, exhibited by many if not all the metals. In fact, elements, M, which form stronger M–M bonds, may well be even better candidates. We have now chosen aluminum for further exploration and describe an ab initio examination of the structure and stabilities of the first examples of hyperaluminum molecules, Al_3O and Al_4O. The former has already been detected among the reaction products of aluminum with oxygen in the gas phase.[20] Matrix isolation and gas-phase investigations of various aluminum–oxygen species also are extensive.[20-38] AlO, AlO_2, Al_2O, Al_2O_2, and AlO_3 have

(16) Würthwein, E.-U.; Schleyer, P. v. R.; Pople, J. A. *J. Am. Chem. Soc.* **1984**, *106*, 6973.
(17) Fallgren, H.; Martin, T. P. *Chem. Phys. Lett.* **1990**, *168*, 233.
(18) Simson, A. *Struct. Bonding (Berlin)* **1979**, *36*, 81.
(19) Borgstedt, H. U. *Top. Curr. Chem.* **1986**, *134*, 125.
(20) Cox, D. M.; Trevor, D. J.; Whetten, R. L.; Rohlfing, E. A.; Kaldor, A. *J. Chem. Phys.* **1986**, *84*, 4651.
(21) Linevski, M. J.; White, D.; Mann, D. E. *J. Chem. Phys.* **1964**, *41*, 542.
(22) Snelson, A. *J. Phys. Chem.* **1970**, *74*, 2574.
(23) Makowiecki, D. M.; Lynch, D. A., Jr.; Carlson, K. D. *J. Phys. Chem.* **1971**, *75*, 1963.
(24) Marino, C. P.; White, D. *J. Phys. Chem.* **1973**, *77*, 2929.
(25) Lynch, D. A., Jr.; Zehe, M. J.; Carlson, K. D. *J. Phys. Chem.* **1974**, *78*, 236.
(26) Finn, P. A.; Gruen, D. M.; Page, D. L. *Adv. Chem. Ser.* **1976**, *No. 158*, 30.
(27) Zehe, M. J.; Lynch, D. A., Jr.; Kelsall, B. J.; Carlson, K. D. *J. Phys. Chem.* **1979**, *83*, 656.
(28) Kelsall, B. J.; Carlson, K. D. *J. Phys. Chem.* **1980**, *84*, 951.
(29) Sonchik, S. M.; Andrews, L.; Carlson, K. D. *J. Phys. Chem.* **1983**, *87*, 2004.
(30) Bares, S. J.; Haak, M.; Nibler, J. W. *J. Chem. Phys.* **1985**, *82*, 670.
(31) Maltsev, A. A.; Shevelkov, V. F. *Tepl.fiz. Vys. Temp., Acad. Nauk SSSR* **1964**, *2*, 650.
(32) Jarrold, M. F.; Bower, J. E. *J. Chem. Phys.* **1986**, *85*, 5373.
(33) Jarrold, M. F.; Bower, J. E. *J. Chem. Phys.* **1987**, *87*, 1610.

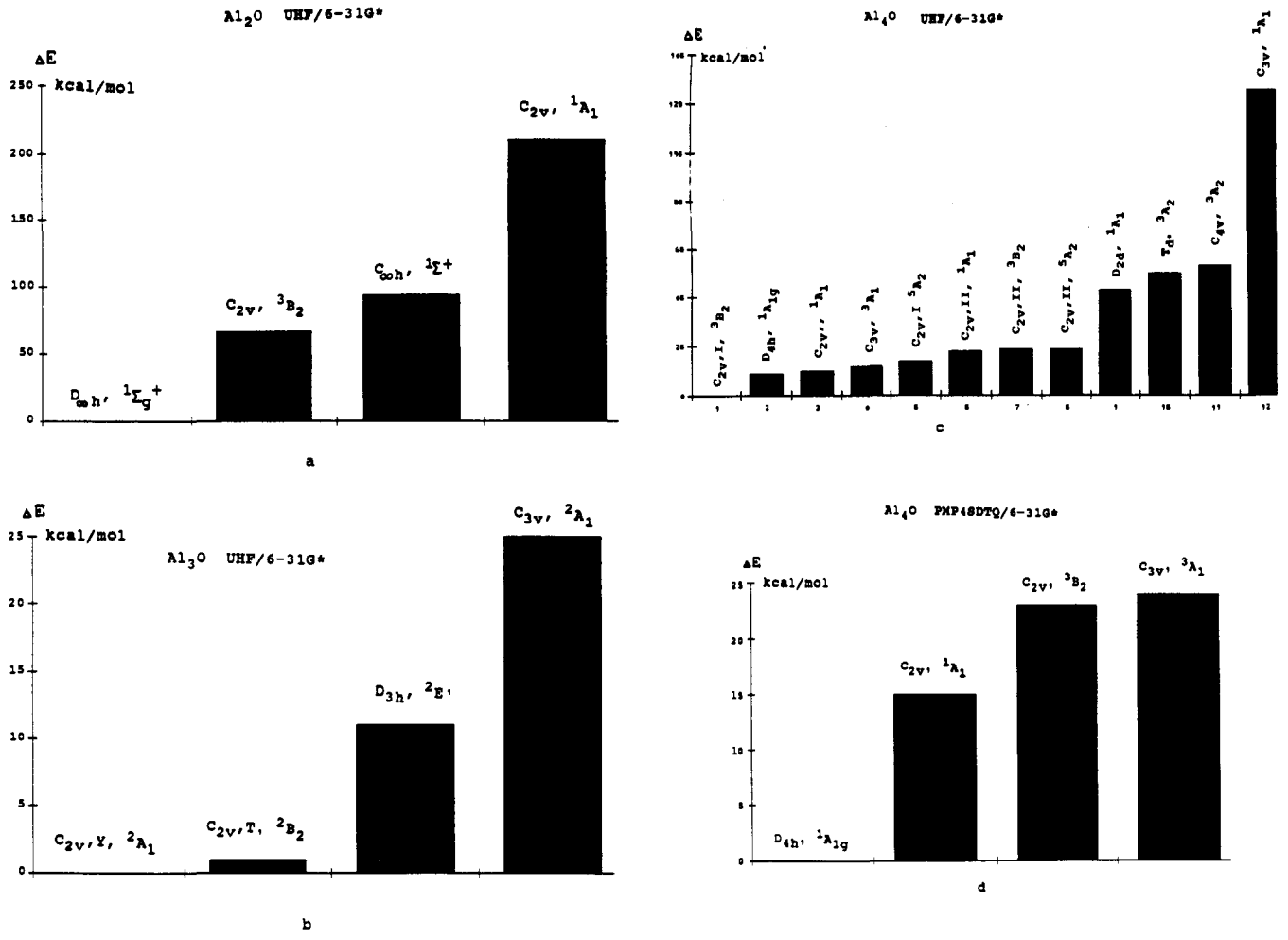

Figure 2. Relative energies of the different forms of Al_2O (a), Al_3O (b), Al_4O (c) at HF/6-31G*, and Al_4O (d) at MP4SDTQ/6-31G*.

Table I. Experimental and Calculated Dissociation Energies at Different Approximations Reaction Energies (kcal/mol)

reaction	PUHG/ 6-31G*	UMP2(full)/ 6-31G*	PMP2/ 6-31G*	PMP3/ 6-31G*	PMP4/ 6-31G*	PMP2/ 6-311+G*	PMP3/ 6-311+G*	PMP4/ 6-311+G*	PMP4+ZPE/ 6-311+G*	expt
1	2	3	4	5	6	7	8	9	10	11
$AlO \rightarrow Al + O$	+52.3	+97.2	+98.1	+89.6	+96.5	+101.7	+91.3	+100.8	+100.3	+121.5 ± 0.9[a]
$Al_2 \rightarrow Al + Al$	+14.2	+26.9	+25.7	+26.8	+28.0	+25.9	+27.0	+28.3	+27.2	+35.7 ± 1.0[a]
$Al_2^+ \rightarrow Al + Al^+$	+26.6	+28.6	+30.2	+29.8	+30.1	+31.1	+30.7	+31.0	+30.8	+20.8 ± 6.9[b]
$Al_2O \rightarrow AlO + Al$	+114.1	+150.0	+143.2	+137.1	+137.4	+142.5	+137.1	+138.0	+136.1	+127.6 ± 2.0[a]
$Al_2O \rightarrow Al_2 + O$	+152.3	+217.9	+215.6	+199.9	+205.9	+218.2	+201.5	+210.4	+209.1	+210.3 ± 4.0[a]
$Al_3^+ \rightarrow Al_2 + Al^+$	+3.1	+36.7	+34.5	+29.4	+31.9	+35.0	+29.9	+32.6	+32.2	+30.0 ± 8.1[c]
$Al_3^+ \rightarrow Al_2^+ + Al$	-13.7	+35.0	+30.1	+26.4	+29.8	+29.8	+26.1	+29.9	+28.7	+25.8 ± 8.1[c]
$Al_3O^+ \rightarrow Al_2O + Al^+$	+27.8	+37.6	+36.3	+37.1	+37.7	+33.5	+34.0	+34.7	+34.1	
$Al_3O \rightarrow Al_2O + Al$	+13.3	+20.9	+21.8	+20.5	+22.1	+19.9	+18.6	+20.3	+19.9	
$Al_3O \rightarrow Al_2 + AlO$	+115.1	+141.6	+139.3	+130.7	+131.5	+136.4	+128.8	+130.0	+128.6	
$Al_4^{2+} \rightarrow Al_3^+ + Al^+$	-54.7									
$Al_4O \rightarrow Al_3O + Al$	+6.8	+52.2	+47.4	+44.0	+47.6	+45.6	+42.6	+46.0	+45.5	
$Al_4O \rightarrow Al_2O + Al_2$	+5.9	+46.2	+43.5	+37.8	+41.7	+39.5	+34.3	+38.0	+37.1	

[a] Reference 50. [b] Reference 70. [c] Reference 61.

been identified.[22,29] In the gas phase, Al_2O, Al_3O,[20] and Al_nO_m (n = 2–26; m = 1, 2) have been demonstrated by mass spectrometry.[32-35] Ab initio calculations are available for AlO,[38] Al_2O,[39-41] Al_2O_2, AlO_2, and AlO_3.[40]

Despite the experimental detection of Al_3O,[20] neither structural nor energetic data are available. We have not been able to find any mention of Al_4O in the literature.

Computational Methods

Geometries of Al_2, Al_2^+, AlO, Al_2O, Al_3O^+, Al_3O, Al_3^+, Al_4^{2+}, and Al_4O were optimized by employing analytical gradients[42] using a polarized split-valence basis set (6-31G*)[43,44] at HF and at correlated MP2(full) levels (UHF and UMP2(full) for open-shell systems). Ge-

(34) Ruatta, S. A.; Hanley, L.; Anderson, S. L. *Chem. Phys. Lett.* **1987**, *137*, 5.
(35) Jarrold, M. F.; Bower, J. E. *J. Chem. Phys.* **1987**, *87*, 5728.
(36) Ruatta, S. A.; Anderson, S. L. *J. Chem. Phys.* **1988**, *89*, 273.
(37) Ovchinnikov, I. V.; Serebrennikov, L. A.; Maltsev, A. A. *Zh. Fiz. Khim.* **1985**, *59*, 1558.
(38) Lengsfield, B. H.; Liu, B. *J. Chem. Phys.* **1982**, *77*, 6083.
(39) Wagner, E. L. *Theor. Chim. Acta* **1974**, *32*, 295.
(40) Masip, J.; Clotet, A.; Ricart, J. M.; Illas, F.; Rubio, J. *Chem. Phys. Lett.* **1988**, *144*, 373.
(41) Solomonik, V. G.; Sazonova, I. G. *Zh. Neorg. Khim.* **1985**, *30*, 1939.
(42) Schlegel, H. B. *J. Comput. Chem.* **1982**, *3*, 214.
(43) Hariharan, P. C.; Pople, J. A. *Theor. Chim. Acta* **1973**, *28*, 213.
(44) Frisch, M. J.; Pople, J. A.; Binkley, J. S. *J. Chem. Phys.* **1984**, *80*, 3265.

Table II. Calculated Frequencies (cm^{-1}) and Zero-Point Energies (ZPE, kcal/mol) of the Aluminum Oxide Species

species symmetry		UHF/ 6-31G*		UMP2(full)/ 6-31G*	species symmetry		UHF/ 6-31G*		UMP2(full)/ 6-31G*
1	2	3	4	5	1	2	3	4	5
AlO ($^2\Sigma^+$)	ω_e	810	(45.7)	789	Al_4^{2+} ($^1A_{1g}$)	ν_4 (e_u)	265		
	ZPE	1.2		1.1	(D_{4h})	ν_5 (b_{2u})	201		
Al_2($^3\Sigma_g^+$)	ω_e	316	(0.0)	366		ZPE	2.4		
	ZPE	0.4		0.5	Al_4O ($^1A_{1g}$)	ν_1 (a_{1g})	390	(0.0)	384
Al_2^+ ($^2\Sigma_g^-$)	ω_e	163	(0.0)	176	D_{4h}	ν_2 (b_{1g})	171	(0.0)	204
	ZPE	0.2		0.3		ν_3 (b_{2g})	287	(0.0)	268
Al_2O ($^1\Sigma_g^+$)	ν_1 (σ_g)	550	(0.0)	513		ν_4 (e_u)	451	(234.4)	538
($D_{\infty h}$)	ν_2 (σ_u)	112	(0.0)	90		ν_5 (e_u)	173	(29.1)	246
	ν_3 (σ_u)	1043	(741.4)	988		ν_6 (a_{2u})	207	(12.5)	157
	ZPE	2.6		2.4		ν_7 (b_{2u})	88	(0.0)	90
Al_2O ($^1\Sigma^+$)	ν_1 (σ)	1195	(53.6)			ZPE	3.4		3.8
($C_{\infty v}$)	ν_2 (σ)	264	(66.3)		Al_4O ($^1A_1$)	ν_1 (a_1)	773	(781.6)	762
	ν_3 (π)	97	(45.5)		C_{2v}, I	ν_2 (a_1)	470	(9.3)	423
	ZPE	2.4				ν_3 (a_1)	274	(9.4)	284
Al_2O ($^1A_1$)	ν_1 (a_1)	764	(60.1)			ν_4 (a_1)	214	(25.6)	233
(C_{2v})	ν_2 (a_1)	426	(16.0)			ν_5 (b_1)	379	(14.3)	401
	ν_3 (b_1)	424	(105.8)			ν_6 (b_1)	150	(0.0)	159
	ZPE	2.3				ν_7 (b_1)	22	(12.0)	92i
Al_3^+ ($^1A_1'$)	ν_1 (a_1')	257	(0.0)	382		ν_8 (b_2)	190	(0.6)	137
(D_{3h})	ν_2 (e')	252	(14.4)	317		ν_9 (b_2)	54	(1.6)	24
	ZPE	1.1		1.5		ZPE	3.6		3.5
Al_3^+ ($^1\Sigma_g^+$)	ν_1 (σ_g)	156	(0.0)	161	Al_4O ($^1A_1$)	ν_1 (a_1)	1037	(840.7)	
($D_{\infty h}$)	ν_2 (σ_u)	259	(190.3)	272	c_{2v}, II	ν_2 (a_1)	541	(6.5)	
	ν_3 (π_u)	78	(0.1)	62		ν_3 (a_1)	216	(3.4)	
	ZPE	0.8		0.8		ν_4 (a_1)	59	(6.8)	
Al_3O^+ ($^1A_1'$)	ν_1 (a_1')	403	(0.0)	385		ν_5 (b_1)	329	(3.7)	
(D_{3h})	ν_2 (e')	509	(291.3)	514		ν_6 (b_1)	135	(11.1)	
	ν_3 (e')	168	(7.8)	146		ν_7 (b_1)	47	(1.3)	
	ν_4 (a_2'')	235	(1.1)	205		ν_8 (b_2)	153	(22.5)	
	ZPE	2.9		2.7		ν_9 (b_2)	74	(4.3)	
Al_3O ($^2A_1$)	ν_1 (a_1)	759	(540.9)	740		ZPE	3.7		
(C_{2v},Y)	ν_2 (a_1)	421	(7.1)	403	Al_4O ($^1A_1$)	ν_1 (a_1)	370		
	ν_3 (a_1)	233	(1.6)	334	D_{2d}	ν_2 (a_1)	228		
	ν_4 (b_1)	170	(4.3)	213		ν_3 (b_1)	172i		
	ν_5 (b_2)	326	(1.8)	139		ν_4 (e)	262		
	ν_6 (b_2)	86	(10.5)	76i		ν_5 (e)	36i		
	ZPE	2.9		2.6		ν_6 (b_2)	330		
Al_3O ($^2B_2$)	ν_1 (a_1)	450		429		ν_7 (b_2)	161i		
(C_{2v},T)	ν_2 (a_1)	383		397		ZPE	2.1		
	ν_3 (a_1)	146		153	Al_4O ($^3A_1$)	ν_1 (a_1)	352	(0.0)	
	ν_4 (b_1)	169		164	T_d	ν_2 (e)	128	(0.0)	
	ν_5 (b_2)	661		643		ν_3 (t_2)	527	(554.0)	
	ν_6 (b_2)	149i		102		ν_4 (t_2)	202	(2.1)	
	ZPE	2.6		2.7	Al_4O ($^3A_1$)	ν_1 (a_1)	459	(4.1)	
Al_4^{2+} ($^1A_1$)	ν_1 (a_1)	75			C_{3v}, I	ν_2 (a_1)	210	(46.5)	
(T_d)	ν_2 (e)	46				ν_3 (a_1)	196	(7.1)	
	ν_3 (t_2)	33				ν_4 (e)	441	(14.5)	
	ZPE	0.4				ν_5 (e)	157	(5.3)	
Al_4^{2+} ($^1A_{1g}$)	ν_1 (a_{1g})	396				ν_6 (e)	52	(4.5)	
(D_{4h})	ν_2 (b_{1g})	735i							
	ν_3 (b_{2g})	533							

[a] IR intensities (KM/mol) are given in parentheses.

ometries of Al_2O ($D_{\infty h}$) and Al_3O (C_{2v}, T) were optimized also at MP2(full)/6-31+G*, but the resulting bond lengths (R(Al–O) = 1.742 Å in Al_2O; $R(Al_1–O)$ = 1.997 Å, $R(Al_2–O) = R(Al_3–O)$ = 1.839 Å in Al_3O) and valence angle ($\angle Al_1OAl_2$ = 99.3° in Al_3O) changed only by 0.02 Å and 0.5°, respectively, from those at MP2(full)/6-31G*. The results are summarized in Figure 1, which includes the experimental distances for AlO and Al_2. Fundamental frequencies, normal coordinates, and zero-point energies (ZPE) were calculated by using standard FG matrix methods. The MP2(full)/6-31G* equilibrium geometries were used to evaluate electron correlation corrections in the frozen-core approximation by Moller–Plesset perturbation theory to full fourth order[45] using 6-31G* and 6-311+G* basis sets (MP4SDTQ/6-31G* and MP4SDTQ/6-311+G*). The UHF wave functions for open-shell systems were projected to pure spectroscopic states (PUHF, PMP2, PMP3, and PMP4).[46] The (U)QCISD(T) level[47] was employed for some of the species as well. Optimizations and analytical frequency calculations at HF/6-31G* and at MP2(full)/6-31G* were carried out with the *CADPAC* Program.[48] *GAUSSIAN 88* (*CONVEX* version) was used to obtain the PMP2, PMP3, PMP4SDTQ, and QCISD data and for the natural population analysis.[49] The total energies at HF/6-31G* and at different correlated levels are given in Tables 1S and 2S. Relative energies of the different forms of Al_2O, Al_3O, and Al_4O at UHF/6-31G* and Al_4O at MP4SDTQ/6-31G* are presented on Figure 2. Dissociation energies and harmonic frequencies are given in Tables I and II, respectively.

Results

Evaluation of the stabilities of Al_3O and Al_4O requires data for Al, O, AlO, Al_2, Al_2^+, and Al_2O. The Al_2^+, Al_3^+, Al_3O^+, and Al_4^{2+} cations also were examined to help understand the nature

(45) Krishnan, R.; Pople, J. A. *Int. J. Quantum Chem.* **1978**, *14*, 91.
(46) Schlegel, H. B. *J. Chem. Phys.* **1986**, *84*, 4530.
(47) Pople, J. A.; Head-Gordon, M.; Raghavachari, K. *J. Chem. Phys.* **1987**, *87*, 5968.
(48) *CADPAC*. Amos, R. D.; Rice, J. E. *CADPAC: The Cambridge Analytic Derivatives Package*, Issue 4.0; Cambridge, 1987.
(49) *GAUSSIAN 88* (*CONVEX* version). Frisch, M. J.; Head-Gordon, M.; Schlegel, H. B.; Raghavachari, K.; Binkley, J. S.; Gonzales, C.; DeFrees, D. J.; Fox, D. J.; Whiteside, R. A.; Seeger, R.; Melius, C. F.; Baker, J.; Martin, R.; Kahn, L. R.; Stewart, J. J. P.; Fluder, E. M.; Topiol, S.; Pople, J. A. Gaussian Inc.: Pittsburgh, PA, 1988.

of the bonding in Al_3O and Al_4O. We describe our results on these reference systems first.

Neutral AlO. The ground state of AlO is known to be $X^2\Sigma^+$[50] with an equilibrium distance of 1.6179 Å, an equilibrium frequency ω_e = 979.23 cm^{-1}, and energy of dissociation $D_0°$ = 121.5 ± 0.9 kcal/mol. We optimized the geometry of AlO ($^2\Sigma^+$) ($(1\sigma)^2(2\sigma)^2(1\pi)^4(3\sigma)^1$ valence configuration) at UHF/6-31G* and at UMP2(full)/6-31G*. Appreciable spin contamination was found at both levels ($\langle S^2\rangle$ = 0.79). Spin-projecting the wave function to the pure spectroscopic state, $^2\Sigma^+$ ($\langle S^2\rangle$ = 0.750), reduced the total energy of AlO modestly, e.g., by 0.0046 au at PMP2/6-31G*. At UMP2(full)/6-31G*, the Al–O bond length (1.648 Å, Figure 1) is longer, and the harmonic frequency (789 cm^{-1}, Table II) is smaller, than experiment. The electron correlation correction to the dissociation energy is quite large, 40–50 kcal/mol; this value oscillated along the PMP2–PMP3–PMP4 series. At PMP4SDTQ/6-311+G*//MP2(full)/6-31G* + ZPE, the calculated D_0 is 20.6 kcal/mol and at QCISD(T)/6-311+G* 14.2 kcal/mol lower than the experimental value. The use of the experimental AlO distance has a negligible effect. Adding a second set of d-functions and one set of f-functions to the basis only improves the calculated D_0 to 113.5 kcal/mol ((U)QCISD(T)/6-311+G(2df)//MP2(full)/6-31G* + ZPE at the experimental geometry).

Neutral Al_2. Dialuminum, Al_2, has already been studied very carefully.[51-58] According to the most extensive CASSCF–SOCI calculations with very large basis sets and relativistic corrections, the $^3\Sigma_g^-$ ($(1\sigma_g)^2(1\sigma_u)^2(2\sigma_g)^1(2\sigma_u)^1$) state lies 174 cm^{-1} (0.6 kcal/mol) above the $^3\Pi_u$ ($(1\sigma_g)^2(1\sigma_u)^2(2\sigma_g)^1(1\pi_u)^1$) ground state.[52]

Aluminum clusters offer challenges for quantum chemistry. SCF convergence is often difficult to achieve, or leads to excited states. Open-shell states at UHF exhibit considerable spin contamination. Moreover, the potential energy surface for open-shell systems may not be smooth at both UHF and PUHF levels (see discussion in ref 59). We have chosen to employ the $^3\Sigma_g^-$ state for Al_2 as our reference; convergence is achieved easily and spin contamination is insignificant (e.g., at UHF/6-31G* $\langle S^2\rangle$ = 2.025). The 0.6-kcal/mol difference in energy between the $^3\Sigma_g^-$ and the ground $^3\Pi_u$ states is negligible. Hence, correction of the dissociation energy estimates for Al_3O and Al_4O is hardly necessary (the inaccuracies in our D_e estimates are larger). The bond length of Al_2 ($^3\Sigma_g^-$) at UMP2(full)/6-31G* (2.469 Å) is very close to the experimental value (2.466 Å, Figure 1). Inclusion of correlation energy is essential to obtain reliable data for the calculated bond length, frequency, and dissociation energy of Al_2 ($^3\Sigma_g^-$).

The Al_2^+ Cation. The Al_2^+ ion has been well studied experimentally[60-64] and theoretically.[56,65,66] All ab initio calculations predict $X^2\Sigma_g^+$ ($(4\sigma_u)^2(5\sigma_g)^1$) ground electronic state. Sunil and Jordan[65] obtained at CCD+ST(CCD)/[12s9p3d1f/6s5p3d1f] 3.208-Å bond length, 169-cm^{-1} equilibrium frequency, and 31.6-kcal/mol dissociation energy for Al_2^+ ($^2\Sigma_g^+$), as well as 6.19- and 5.92-eV vertical and adiabatic first ionization potentials (IP) for Al_2 ($X^3\Pi_u$). Bauschlicher et al.[66] at CASSCF/SOCI/[20s13p6d4f/6s5p3d2f] obtained similar results: r_e = 3.212 Å, ω_e = 169 cm^{-1}, and D_e = 32.7 kcal/mol for Al_2^+($^2\Sigma_g^+$) and IP_{vert} = 6.14 eV and IP_{ad} = 5.90 eV for Al_2($X^3\Pi_u$). These theoretical values may be compared with the available experimental data for Al_2^+: ω_e = 178.8 cm^{-1},[62] and D_0 = 20.8 ± 6.9 kcal/mol[61] and $IP_{ad}(Al_2)$ = 5.989 ± 0.002 eV.[64] There is good agreement between theoretical and experimental data ($D_0(Al_2^+)$ is an exception but the experimental value needs to be refined). Our calculated r_e = 3.138 Å and ω_e = 176 cm^{-1} at UMP2(full)/6-31G* and D_0(Al_2^+, $^2\Sigma_g^+$) = 30.8 kcal/mol as well as $IP_{ad}(Al_2, {}^3\Pi_g^+)$ = 5.6 eV (both at PMP4SDTQ/6-311+G*//MP2(full)/6-31G* + ZPE) agree reasonably well with the best ab initio and experimental data.

Neutral Al_2O. Molecular Al_2O has also been investigated experimentally[22,29,31,37,57] and theoretically.[39-41] Gas-phase IR measurements[31,37] indicate Al_2O to be linear $D_{\infty h}$, but matrix isolation experiments[57] were interpreted in favor of a bent C_{2v} geometry. Both of these structures have been considered theoretically;[39-41] geometry optimization at the HF/DZ and the HF/DZ+P levels led to a linear $D_{\infty h}$ ($^1\Sigma_g^+$) structure, whatever bond angle was assumed initially. We have examined three basic forms: linear Al–O–Al ($D_{\infty h}$), linear Al–Al=O ($C_{\infty v}$), and angular Al–O–Al (C_{2v}), all in singlet and triplet states. Both linear structures should have closed-shell singlet ground electronic states. Linear AlOAl has a $(1\sigma_g)^2(1\sigma_u)^2(1\pi_u)^4(2\sigma_g)^2(2\sigma_u)^2(1\pi_g)^0$ valence configuration. In the corresponding triplet state, the $1\pi_g$–MO would be occupied by only one electron, and Jahn–Teller distortion to bent forms is expected. For similar reasons the $C_{\infty v}$ structure ($(1\sigma)^2(2\sigma)^2(3\sigma)^2(1\pi)^4(4\sigma)^2(2\pi)^0$ valence configuration) also should be a singlet.

We find the $D_{\infty h}$ ($^1\Sigma_g^+$) structure to be the Al_2O global minimum. While the $C_{\infty v}$ ($^1\Sigma^+$) form is a local minimum, it is 94.1 kcal/mol higher in energy at HF/6-31G*. Nevertheless, this structure also is thermodynamically stable with respect to dissociation into AlO + Al and may be detectable in matrix isolation experiments.

Starting with a 120° AlOAl angle, HF/6-31G* geometry optimization in C_{2v} symmetry led to the linear, $D_{\infty h}$ structure. But a 60° starting angle resulted in a local minimum with an equilibrium angle of 78.2°. This ($^1A_1$) singlet state has the $(1a_1)^2(2a_1)^2(1b_2)^2(1b_1)^2(3a_1)^2(2b_1)^2(2b_2)^0$ valence configuration. Similarly, a 91.5° angle was found for the ($^3B_2$) triplet state with the $(1a_1)^2(2a_1)^2(1b_2)^2(1b_1)^2(3a_1)^2(4a_1)^1(2b_2)^1$ configuration. The C_{2v} ($^3B_2$) structure lies 66.8 kcal/mol above the ground state; the relative energy of C_{2v} ($^1A_1$) is even higher, 211.0 kcal/mol at HF/6-31G*. At this uncorrelated level, the stability of the four isomers is: $D_{\infty h}$ ($^1\Sigma_g^+$) < $C_{\infty v}$($^1\Sigma^+$) < C_{2v}($^3B_2$) < C_{2v}($^1A_1$) (see Figure 2a).

Our calculated frequencies at HF/6-31G* for the linear $D_{\infty h}$ form (see Table IV) correspond well with the prior theoretical values (531, 129, and 1012 cm^{-1} [40] and 527, 102, and 1057 cm^{-1} [39]); our calculated Al–O bond length also agrees.[39-41] The frequencies calculated analytically at MP2(full)/6-31G* 513, 90, and 988 cm^{-1} are even closer to the available experimental data 472, 100, and 992 cm^{-1}.[28,37] A correction increases the Al–O bond length 0.03 Å on reoptimization (Figure 1).

Our calculated dissociation energy (MP4SDTQ/6-311+G*//MP2(full)/6-31G* + ZPE) of Al_2O into Al_2 + O, 209.1 kcal/mol, agrees well with the experimental value, 210.3 ± 4.0, but this is not the case for dissociation into AlO + Al. Our best estimate is 8.5 kcal/mol larger than experiment. This reflects our difficulty in reproducing the experimental $D_0°$ (AlO) value (see above).

(50) Huber, K. P.; Herzberg, G. *Molecular Spectra and Molecular Structure. Constants of Diatomic Molecules*; Van Nostrand Reinhold: New York, 1979.
(51) Bauschlicher, C. W., Jr.; Pettersson, L. G. M. *J. Chem. Phys.* **1987**, *87*, 2198.
(52) Bauschlicher, C. W., Jr.; Partridge, H.; Langhoff, S. R.; Taylor, P. R.; Walch, S. P. *J. Chem. Phys.* **1987**, *86*, 7007.
(53) Tse, J. S. *J. Mol. Struct. (THEOCHEM)* **1988**, *165*, 21.
(54) Basch, H.; Stevens, W. J.; Krauss, M. *Chem. Phys. Lett.* **1984**, *109*, 212.
(55) Ginter, D. S.; Ginter, M. L.; Innes, K. K. *Astrophys. J.* **1964**, *139*, 365.
(56) Upton, T. H. *J. Chem. Phys.* **1987**, *86*, 7054.
(57) Douglas, M. A.; Hauge, R. H.; Margrave, J. L. *J. Phys. Chem.* **1983**, *87*, 2945.
(58) Abe, H.; Kolb, D. M. *Ber. Bunsenges. Phys. Chem.* **1983**, *87*, 523.
(59) Tse, J. S. *J. Chem. Phys.* **1990**, *92*, 2488.
(60) Jarrold, M. F.; Bower, J. E.; Kraus, J. S. *J. Chem. Phys.* **1987**, *86*, 3876.
(61) Hanley, L.; Ruatta, S. A.; Anderson, S. L. *J. Chem. Phys.* **1987**, *87*, 260.
(62) Cox, D. M.; Trevor, D. J.; Whetten, R. L.; Kaldor, A. *J. Phys. Chem.* **1988**, *92*, 421.
(63) Fuke, K.; Nonose, S.; Kikuchi, N.; Kaya, K. *Z. Phys.* **1989**, *D12*, 571.
(64) Harrington, J. E.; Weisshaar, J. C. *J. Chem. Phys.* **1990**, *93*, 854.
(65) Sunil, K. K.; Jordan, K. D. *J. Phys. Chem.* **1988**, *92*, 2774.
(66) Bauschlicher, C. W., Jr.; Barnes, L. A.; Taylor, P. R. *J. Phys. Chem.* **1989**, *93*, 2932.
(67) Bucher, A.; Stauffer, J. L.; Clemperer, W.; Wharton, L. *J. Chem. Phys.* **1963**, *39*, 2463.

The Al_3^+ Cation. The geometry and electronic structure of the related cation clusters may help to understand the stability of the Al_3O^+ and Al_3O species. The Al_3^+ ion has been detected in mass spectra[61,68] and has been studied theoretically.[69] Hanley et. al.[61] reported dissociation energies of Al_3^+ (into $Al_2 + Al^+$) of 30.0 ± 8.1 kcal/mol and (into $Al_2^+ + Al$) of 25.8 ± 8.1 kcal/mol. Basch calculated the equilibrium geometries for several states.[69] Three of these were linear and were described as "singlet $^1A_1$ $((1a_1)^2(2a_1)^2(1b_1)^2(2b_1)^2)$", "triplets $^3B_1$ $((1a_1)^2(2a_1)^2(1b_1)^2(2b_1)^1(3a_1)^1)$", and "triplet $^3A_2$ $((1a_1)^2(2a_1)^2(1b_1)^2(2b_1)^1(1b_2)^1)$". In addition, a "triplet $^3B_2$ $((1a_1)^2(2a_1)^2(1b_1)^2(1b_2)^1(3a_1)^1)$" possessed a strongly bent structure. However, the "$^3B_1$" and "$^3A_2$" triplets in ref 69 only are representations of the same $^3\Pi_g$ wave function; indeed, the calculated energies of these "states" are reported to be identical. The linear $D_{\infty h}$ ($^1\Sigma_g^+$) $((1\sigma_g)^2(1\sigma_u)^2(2\sigma_g)^2(2\sigma_u)^2(1\pi_u)^0$ valence configuration) form was found to be the most stable with a calculated dissociation energy, Al_3^+ ($^1\Sigma_g^+$) → Al_2^+ ($^2\Sigma_g^+$) + Al(^{2}P), of 39.2 kcal/mol.

We examined Al_3^+ in D_{3h} and $D_{\infty h}$ symmetries (both as singlets and as triplets). Misleadingly, HF/6-31G* optimization gives the linear $D_{\infty h}$ ($^1\Sigma_g^+$) structure (as was found in ref 69 at the CAS MC SCF level), but with the larger 6-311+G* basis set and with electron correlation we found the triangular D_{3h} ($^1A_1'$) $((1a_1')^2(1e')^4(1a_2'')^2(2e')^0$ valence configuration) to be favored. The linear $D_{\infty h}$ ($^1\Sigma_g^+$) structure is 31.3 kcal/mol higher in energy at MP4SDTQ/6-311+G*//MP2(full)/6-31G*. The other singlet linear structures with $(1\sigma_g)^2(1\sigma_u)^2(1\pi_u)^4(2\sigma_g)^0$ and $(1\sigma_g)^2(1\sigma_u)^2(2\sigma_g)^2(1\pi_u)^2(2\sigma_u)^0$ electronic configurations are much higher in energy. Similarly, the linear triplets with $(1\sigma_g)^2(1\sigma_u)^2(2\sigma_g)^2(1\pi_u)^2(2\sigma_u)^0$ and $(1\sigma_g)^2(1\sigma_u)^2(2\sigma_g)^2(1\pi_u)^1(2\sigma_u)^1$ electronic configurations as well as bent C_{2v} triplet $((1a_1)^2(2a_1)^2(1b_1)^2(1b_2)^1(3a_1)^1)$ lie more than 25 kcal/mol above the ground state at HF/6-31G*. The Al_3^+ cation has a D_{3h} ($^1A_1'$) global minimum according to our best calculations.

The calculated dissociation energies for dissociation of Al_3^+ (D_{3h}) into $Al_2 + Al^+$, 29.9 kcal/mol, and into $Al_2^+ + Al$, 31.0 kcal/mol, agree well with the experimental data, 30.0 ± 8.1 and 25.8 ± 8.1 kcal/mol, respectively.[61] Correlation corrections (which amount to 30 kcal/mol at MP4SDTQ/6-31G*!) are important for the accurate estimation of the Al_3^+ cation dissociation energy (see Table I).

The Al_3O^+ Cation. The Al_3O^+ cation was detected in the mass spectrum of the reaction product of aluminum cluster ions, Al_k^+, with oxygen.[32,34] Nonetheless, neither the structure nor the electronic state of Al_3O^+ is known. The vibrational spectra and the dissociation energy have also not been determined to our best knowledge.

We investigated two Al_3O^+ structural possibilities, with D_{3h} (the oxygen atom is in the center of the Al_3 triangle) and with C_{3v} symmetry (the oxygen atom is at the vertex of a pyramid). Only the D_{3h} singlet $((1a_1')^2(1e')^4(1a_2'')^2(2a_1')^2(2e')^4(3e')^0$ valence configuration) was found to be a minimum. Optimization in C_{3v} symmetry (starting with a 109° AlOAl angle) led to the D_{3h} planar structure. The D_{3h} structure for Al_3O^+ is expected because of the highly ionic bonding between O^{2-} anion and the three Al^+ cations.

Interestingly, the Al^+ cation affinity of Al_2O is only 5 kcal/mol more than that of Al_2 (MP4SDTQ/6-311+G* + ZPE). We have not examined the Al_3O^+ triplet, but this should not have a planar, trigonal structure. In D_{3h} symmetry, both HOMO and LUMO have e-symmetry. An $(2e^3)(3e^1)$ electronic configuration should lead to Jahn–Teller distortion. The Al_3O^+ triplet state should be higher than singlet because the HOMO–LUMO gap is quite large (9.3 eV).

Neutral Al_3O. While there is mass spectroscopic evidence for Al_3O,[20] no detailed information, e.g., on the structure, frequencies, or energy, is available. The highest possible symmetry, D_{3h}, is not expected for Al_3O since in the $(1a_1')^2(1e')^4(1a_2'')^2(2a_1')^2(2e')^4(3e')^1$ valence configuration only the electron occupies the degenerate 3e HOMO. Jahn–Teller distortion leads to Y-type or T-type geometries, both in C_{2v} symmetry. We designate these (C_{2v},Y) ($^2A_1$: $(1a_1)^2(2a_1)^2(1b_2)^2(1b_1)^2(3a_1)^2(4a_1)^2(2b_1)^2(5a_1)^1$) and ($C_{2v}$,T) ($^2B_2$: $(1a_1)^2(2a_1)^2(1b_2)^2(1b_1)^2(3a_1)^2(4a_1)^2(2b_1)^2(2b_2)^1$). Both were optimized, as were pyramidal (C_{3v}) ($^2A_1$: $(1a_1)^2(1e)^4(2a_1)^2(1a_2)^2(2e)^4(3a_1)^1$) and planar ($D_{3h}$) (^{2}E: $(1a_1')^2(1e'')^4(1a_2'')^2(2a_1)^2(2e')^4(3e')^1$) forms (see Figure 1). Appreciable spin contamination was found for all four structures ($\langle S^2\rangle$ = 0.79–0.85) in the initial examination at HF/6-31G*. After spin-projecting the wave function to pure spectroscopic states, the total energies of these structures of Al_3O decreased by 0.0045–0.0065 au (at PUHF/6-31G*).

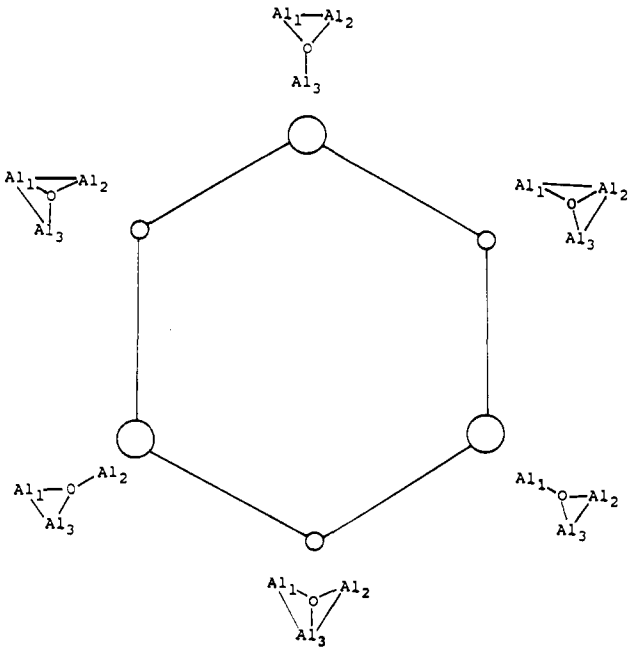

Figure 3. Graph of the Al_3O flexible intramolecular rearrangement.

At this level, the Al_3O C_{2v},Y ($^2A_1$) form is a minimum and the C_{2v},T ($^2B_2$) form is a saddle point on the intramolecular rearrangement (see Figure 3); the C_{3v} ($^2A_1$) isomers is a local minimum, and the D_{3h} (^{2}E) structure is a saddle point second order (two imaginary frequencies). At HF/6-31G* the barrier on the Al_3O intramolecular rearrangement is only 1.4 kcal/mol (1.1 kcal/mol with ZPE correction). As the relative energy of the C_{3v} ($^2A_1$) isomer was quite high, 25.4 kcal/mol at UHF/6-31G*, this portion of the PES was not examined further. The D_{3h} (^{2}E) structure lies 10.9 kcal/mol above the most stable C_{2v},Y ($^2A_1$) form. At the HF/6-31G* level, the stability of the four forms is C_{2v},Y ($^2A_1$) > C_{2v},T ($^2B_2$) > D_{3h} (^{2}E) > C_{3v} ($^2A_1$) (see Figure 2b).

The lowest energy C_{2v},Y, C_{2v},T, and D_{3h} Al_3O structures were reoptimized at MP2(full)/6-31G*, and single points were calculated at MP4SDTQ/6-31G* and at MP4SDTQ/6-311+G* (see Table II and Figure 1). At MP2(full)/6-31G*, the C_{2v},T ($^2B_2$) structure is the global minimum, but the C_{2v},Y ($^2A_1$) saddle point structure is only 1.1 kcal/mol higher in energy. This difference is even smaller (0.5 kcal/mol) at PMP4SDTQ/6-311+G* + ZPE, our highest level. Therefore, the Al_3O molecule is highly flexible with respect to distortion in the plane. A nonrigid model with large amplitude motions of the Al atoms should be used for describing the structure and spectra of this species. The D_{3h} (^{2}E) structure lies 26.4 kcal/mol (MP2(full)/6-31G*) above the global minimum; however, this ^{2}E state (D_{3h} symmetry) may require multiconfiguration treatment for a more reliable estimation of the relative energy.

We have considered only two channels for dissociation of Al_3O into Al_2O + Al and Al_2 + AlO. All other possibilities would

(68) Ray, U.; Jarrold, M. F.; Bower, J. E.; Krauss, J. S. *Chem. Phys. Lett.* **1989**, *159*, 221.
(69) Basch, H. *Chem. Phys. Lett.* **1987**, *136*, 289.
(70) Chase, M. W., Jr.; Davies, C. A.; Downey, J. R., Jr.; Frurip, D. J.; McDonald, R. A.; Syverund, A. N. *JANAF Thermochemical Tables*, 3rd ed.: Parts I and II; *J. Phys. Chem. Ref. Data* **1986**.

require much more energy. (Note that the Al–O bond dissociation energy, 121.5 kcal/mol, is much larger than that of Al–Al, 35.7 kcal/mol.) The data in Table I also show the degree to which Al_3O is stable toward all possible dissociation pathways; this accords with its experimental observation.[20]

The calculated adiabatic IPs of Al_3O ($^2B_2$ and $^2A_1$) are both 5.1 eV at PMP4SDTQ/6-311+G* + ZPE.

The Al_4^{2+} Cation. We consider the Al_4^{2+} cation because of the ionic character of Al_4O: the O^{2-} anion is surrounded by on Al_4^{2+} cage. We optimized singlet Al_4^{2+} in tetrahedral (T_d) $((1a_1)^2(1t_2)^6(2a_1)^2(2t_2)^0$ valence configuration) and in square-planar (D_{4h}) $((1a_{1g})^2(1e_u)^4(1a_{2u})^2(2a_{1g})^2(1b_{1g})^0)$ geometries. The T_d form is a minimum but the D_{4h} form is a saddle point at HF/6-31G* (see Table II). Because of Coulomb repulsion, Al_4^{2+} is not stable thermodynamically toward dissociation.

Neutral Al_4O. The structure of molecular Al_4O cannot be predicted on the basis of classical valence theory. Many possible geometries need to be considered. Our search strategy employed a fragment approach. We divided Al_4O into two sets of closed-shell moieties, $Al_4^{2+} + O^{2-}$ and $AlO^- + Al_3^+$. Different ways of combining these fragments were explored. Thus, the oxygen dianion, O^{2-} may be placed inside a Al_4^{2+} tetrahedron (the most stable Al_4^{2+} structure) or may be coordinated to its face, edge, or vertex. The lower D_{2d} symmetry for Al_4O with oxygen in the center also was considered. Likewise, the oxygen end of the AlO^- fragment may be coordinated to the face, edge, and vertex of the triangular Al_3^+ cation (the most stable Al_3^+ structure). We also optimized geometries for singlet and triplet C_{4v} structures. These pyramidal forms may be considered to be an ionic complexes comprised of a O^{2-} dianion coordinated to a square-planar Al_4^{2+} (D_{4h}) dication. Overall D_{4h} symmetry is possible when the O^{2-} lies in the center of Al_4^{2+} (D_{4h}). All the Al_4O structures which survived after optimization are summarized in Figure 1.

First, consider the possibilities with the O^{2-} inside a Al_4^{2+} "cage". In T_d symmetry, the eight oxygen dianion valence electrons of O^{2-} must interact with the virtual Al_4^{2+} (T_d) MO's of appropriate symmetry. However, only two electrons are available to occupy the doubly degenerate 1e HOMO in Al_4O (T_d) $((1a_1)^2(1t_2)^6(2a_1)^2(2t_2)^6(1e)^2(3t_2)^0$ valence configuration). Hence, Jahn–Teller distortion is expected in the singlet state. (This leads to the (D_{4h}) planar structure on optimization.) The (D_{4h}) singlet ($^1A_{1g}$) $((1a_{1g})^2(1e_u)^4(1a_{2u})^2(2a_{1g})^2(2e_u)^4(1b_{2g})^2(1b_{1g})^2(1e_g)^0$ valence configuration) structure is a minimum at the HF and is the global minimum at our highest, correlated level (see Table II). The (D_{2d}) ($^1A_1$) $((1a_1)^2(1b_2)^2(1e)^4(2a_1)^2(2b_2)^2(2e)^4(3a_1)^2(3b_2)^0$ configuration) is lower in energy that the T_d but has three imaginary frequencies.

The triplet (T_d) ($^3A_1$) state is a minimum since each of the 1e MO's is singly occupied $((1a_1)^2(1t_2)^6(2a_1)^2(2t_2)^6(1e)^2(3t_2)^0$ valence configuration). Nevertheless, this state is 41.4 kcal/mol less stable than the (D_{4h}) singlet at HF/6-31G* and is not a viable form. This energy difference is even larger at correlated levels.

All three structures with O^{2-} coordinated to the face (C_{3v},I), the edge (C_{2v},III), and the vertex (C_{3v},II) of tetrahedral Al_4^{2+} were optimized in singlet and triplet states. The (C_{3v},I) structure is expected to be a triplet, because two electrons are available to occupy the doubly degenerate e HOMO. Indeed, two imaginary frequencies (Table II) are calculated for the singlet C_{3v} form. The C_{3v},I triplet ($^3A_1$) $((1a_1)^2(1e)^4(2a_1)^2(3a_1)^2(2e)^4(4a_1)^2(3e)^2(4e)^0$ valence configuration) is a minimum only 3.2 kcal/mol higher in energy (HF/6-31G*) than the D_{4h} ($^1A_{1g}$) form. Upon optimization of the C_{2v},II states, the singlet led to the D_{4h} minimum and the triplet to the square-pyramidal (C_{4v}) ($^3B_1$) geometry. The C_{3v},II singlet ($^1A_1$) $((1a_1)^2(2a_1)^2(3a_1)^2(1e)^4(2e)^4(4a_1)^2(5a_1)^2(3e)^0$ valence configuration) lies 129.6 kcal/mol above the D_{4h} form at HF/6-31G*.

The third set of Al_4O structure involves AlO^-, Al_3^+ interaction. At HF, the singlet $^1A_1$ $((1a_1)^2(2a_1)^2(1b_2)^2(1b_1)^2(3a_1)^2(4a_1)^2(2b_2)^2(5a_1)^2(6a_1)^2(2b_1)^0)$, triplet $^3B_2$ $((1a_1)^2(2a_1)^2(3a_1)^2(1b_2)^2(1b_1)^2(2b_2)^2(4a_1)^2(2b_1)^2(5a_1)^1(3b_2)^1)$, and quintet $^5A_2$ $((1a_1)^2(2a_1)^2(1b_2)^2(1b_1)^2(3a_1)^2(4a_1)^2(2b_2)^2(5a_1)^1(6a_1)^1(2b_1)^1(3b_2)^1(4b_2)^0)$ states of the C_{2v},I form (in which the AlO^- fragment is coordinated to the edge of the triangular Al_3^+ cation) are low in energy (see Figure 2c). The C_{2v},I ($^3B_2$) triplet is actually the most stable Al_4O species at uncorrelated levels. Of course, correlation favors singlet over triplet states. Thus, the corresponding singlet, C_{2v},I ($^1A_1$), also a minimum, is 10.0 kcal/mol higher in energy than the C_{2v},I ($^3B_2$) triplet at HF/6-31G* but is 6.3 kcal/mol more stable at MP4SDTQ/6-31G*. At MP4SDTQ/6-31G* the C_{2v},I singlet is 21.3 kcal/mol higher in energy than the most singlet D_{4h} form. None of the singlet, triplet, and quintet C_{2v},I structures are competitive energetically. The same is true of planar C_{2v},II forms (which have the AlO^- fragment coordinated to the vertex of the Al_3^+ triangle): the singlet ($^1A_1$) $((1a_1)^2(2a_1)^2(1b_2)^2(1b_1)^2(3a_1)^2(2b_2)^2(4a_1)^2(5a_1)^2(3b_2)^2(2b_1)^0)$, the triplet ($^3B_2$) $((1a_1)^2(2a_1)^2(1b_2)^2(1b_1)^2(3a_1)^2(2b_2)^2(4a_1)^2(5a_1)^2(3b_2)^1(6a_1)^1)$, and the quintet ($^5A_2$) $((1a_1)^2(2a_1)^2(3a_1)^2(1b_2)^2(1b_1)^2(2b_2)^2(4a_1)^2(5a_1)^1(3b_2)^1(6a_1)^1(2b_1)^1(1a_2)^0)$ are 17.7, 18.5, and 19.0 kcal/mol less stable (at HF/6-31G*) than the C_{2v},I ($^3B_2$) minimum.

HF/6-31G* optimization of square-pyramidal Al_4O in C_{4v} symmetry (a $^1A_1$ state starting with the $((1a_1)^2(1e)^4(2a_1)^2(3a_1)^2(2e)^4(1b_2)^2(1b_1)^2(4a_1)^0$ valence configuration) led to the planar D_{4h} ($^1A_{1g}$) structure. Optimization of the alternative $^3B_1$ state also in C_{4v} symmetry (starting with the $(1a_1)^2(1e)^4(2a_1)^2(3a_1)^2(2e)^4(1b_2)^2(1b_1)^1(4a_1)^1(3e)^0$ valence configuration) did result in square-pyramidal structure, but the relative energy was 106.8 kcal/mol.

To summarize, the initial search at HF(or UHF)/6-31G* led to the following energy ordering for the various Al_4O species: C_{2v},I ($^3B_2$) 0.0 < D_{4h} ($^1A_{1g}$) 8.5 < C_{2v},I ($^1A_1$) 10.0 ≈ C_{3v},I ($^3A_1$) 11.8 C_{2v},I ($^5A_2$) 13.5 < C_{2v},II ($^1A_1$) 17.7 ≈ C_{2v},II ($^3B_2$) 18.5 ≈ C_{2v},II ($^5A_2$) 19.0 < D_{2d} ($^1A_1$) 43.2 < T_d ($^3A_1$) 50.0 ≈ C_{4v} ($^3A_2$) 52.1 < C_{3v},II ($^1A_1$) 125.2 (see Figure 2c).

The lowest energy forms were selected for refinement and were reoptimized at MP2(full)/6-31G* (Figure 2d). Electron correlation correction is known to favor singlets over triplets, and also more compact structures. Indeed, at MP2(full)/6-31G* the square-planar (D_{4h}) ($^1A_{1g}$) form is the global minimum. Both C_{2v} singlets, I and II, are higher in energy (18.7 and 42.3 kcal/mol, respectively), and neither one is a minimum at MP2(full)/6-31G*. The C_{2v},I triplet, which was the lowest energy Al_4O form at HF/6-31G*, lies 21.3 kcal/mol above the D_{4h} singlet at PMP4SDTQ/6-31G* (calculated using the UHF/6-31G* geometry). The relative energy of the triplet C_{3v},I structure is 24.4 kcal/mol at PMP4SDTQ/6-31G*//HF/6-31G*.

Our best estimates of the final relative energies (at PMP4SDTQ/6-31G*) are (in kcal/mol): D_{4h} ($^1A_{1g}$) 0.0 < C_{2v},I ($^1A_1$) 15.0 < C_{2v},I ($^3B_2$) 21.3 < C_{3v},I ($^3A_1$) 24.4. Hence, we predict that Al_4O favors the unusual square-planar (D_{4h}, $^1A_{1g}$) structure rather strongly. Our calculated frequencies at MP2(full)/6-31G* (Table II) may help identification in the gas phase and in the matrix isolation.

Bonding and Structure of the Aluminum Oxides

Natural population and natural bond orbital analyses[71,72] of the various aluminum oxide species are summarized in Figure 4. The systems are categorized into two group. The Al–O bonds in the first group (AlO, Al_2O ($D_{\infty h}$), and Al_3O^+) are essentially fully ionic. Note the large values of the natural charges. Furthermore, the nonorthogonal Wiberg overlap populations (a measure of the covalent contributions) between the central atom and the ligands and especially between the ligands are very small. Therefore, the chemical bonding in this group is not unusual; the chief attractive interactions, largely electrostatic, are between the central oxygen atom and the aluminum ligands.

According to classical theories of valence, neither Al_3O nor Al_4O should be stable because the maximum "combining capacity" of oxygen is two. Even so, the nature of the Al_3O^+ cation is not hard to understand. Aluminum is a very electropositive element (the electronegativity is 1.47 on the Allred–Rochow scale). Like H_3O^+ and especially Li_3O^+, Al_3O^+ is a highly ionic complex in which three monovalent Al^+ cations interact with an O^{2-} dianion. The

(71) Reed, A. E.; Weinhold, F. *QCPE Bull.* **1985**, *5*, 141.
(72) Reed, A. E.; Weinhold, F. *Chem. Rev.* **1988**, *88*, 899.

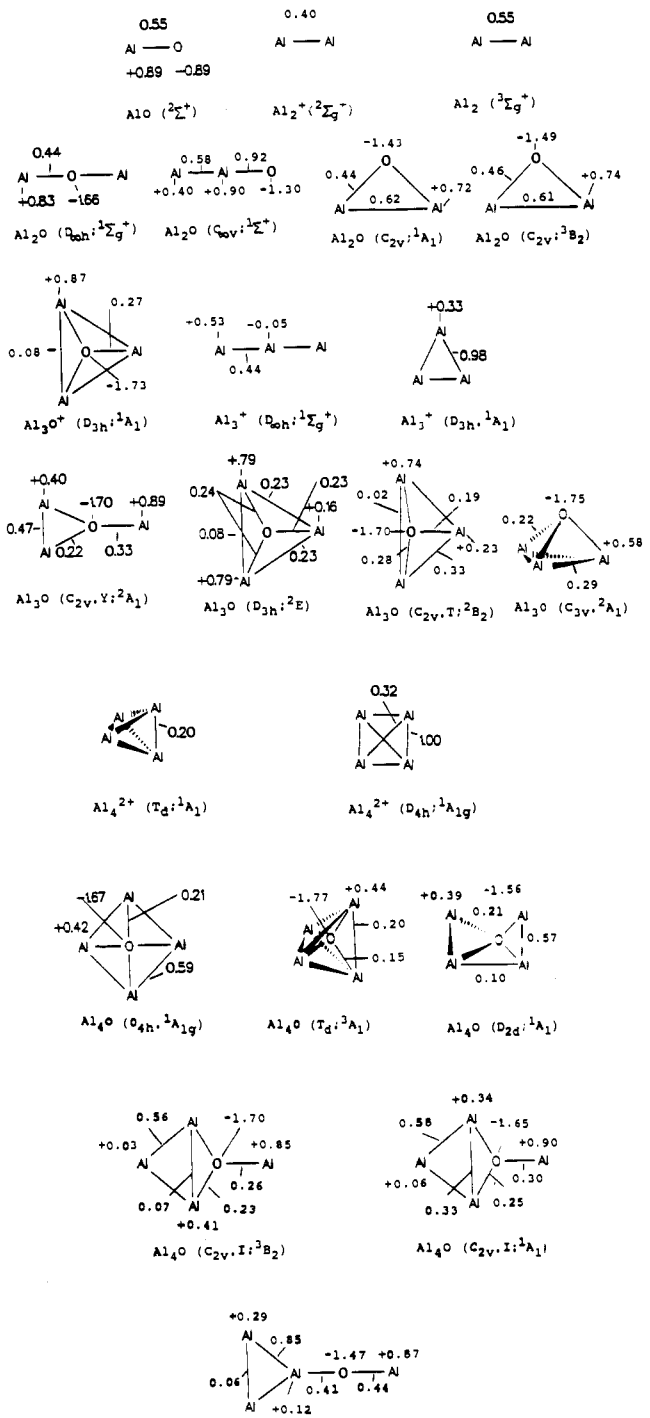

Figure 4. Natural charges and nonorthogonal natural atomic overlap populations of aluminum oxides (HF/6-31G*).

bonding in the neutral Al_2O molecule is similar: $Al^+O^{2-}Al^+$. The preference of Al_2O for linear, and Al_3O^+ for a planar, trigonal geometry is due to the predominant electrostatic repulsion of the Al^+ ligands. Even though each Al^+ cation has two valence electrons at its disposal, the central oxygen atom octet already is "saturated" and Al–Al bonding cannot compete effectively. Some Al–Al bonding is present in the bent forms of Al_2O, but these are much higher in energy.

The bonding situation in Al_3O and Al_4O is significantly different. As the oxygen retains its 2- character (a higher negative charge is unrealistic), the aluminum charges are reduced from the ca. 1+ values in Al_2O and Al_3O^+. Hence, the electrostatic ligand–ligand repulsion is less important, and Al–Al bonding can contribute more effectively. The stability of both Al_3O and Al_4O is due to the attractive interactions among the ligands. This also is the case, but to a lesser extent, in the hypermetalated molecules

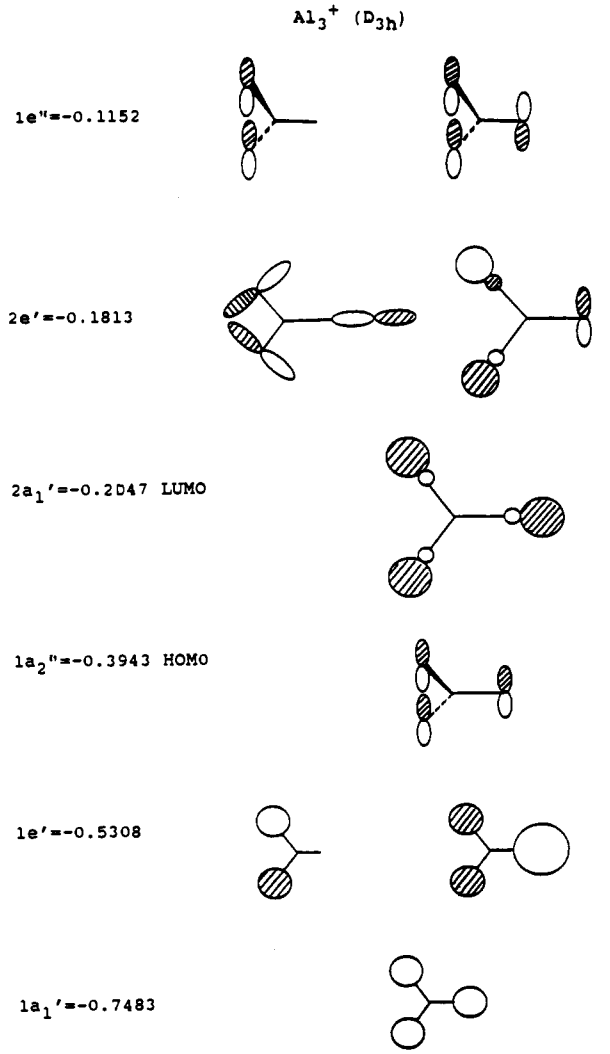

Figure 5. MO scheme of Al_3^+ (D_{3h}).

involving lithium, sodium, etc.[1-6] As shown in Figure 4, all stable Al_3O and Al_4O structures benefit from relatively large overlap (nonorthogonal) populations between aluminum atoms. The reference data provided for the polyaluminum species, Al_2, Al_2^+, Al_2^{2+}, Al_3^+ (D_{3h}), and Al_4^{2+} (T_d), provide calibration. Note that the C_{2v},Y structure of Al_3O can be interpreted as a triple ion: a monovalent Al^+ cation and a Al_2^+ radical cation interacting with O^{2-}. The possible alternative C_{3v} arrangement, in which O^{2-} would interact with a triangular Al_3^{2+} cation, would not reduce the electrostatic repulsion as effectively. The same interpretation rationalizes the stability of the D_{4h} Al_4O versus the other possible forms.

Examination of the molecular orbitals also helps clarify why some of these molecules have bonding ligand–ligand interactions while others do not. Figures 5 and 6 provide qualitative MO schemes for the Al_3^+ and Al_3O^+ cations. The MO's of Al_3O^+ can be derived from the Al_3^+ (D_{3h}) MO's and O^{2-} AO's: $1a_1'$-MO ($1a_1'$-MO(Al_3^+) + 2s(O^{2-})), 1e'-MO (1e'(Al_3^+) + $2p_x$,$2p_y$(O^{2-})), $1a_2''$-MO ($1a_2''(Al_3^+)$ + $2p_z(O^{2-})$), $2a_1'$-MO ($1a_1'(Al_3^+)$ - 2s-(O^{2-})), 2e'-HOMO (1e'(Al_3^+) - $2p_x$,$2p_y$(O^{2-})), 3e'-LUMO (2e'(Al_3^+) + $2p_x(O^{2-})$ and 2e'(Al_3^+) - $2p_y(O^{2-})$), $2a_2''$-MO ($1a_2''(Al_3^+)$ - $2p_z(O^{2-})$). Both 1e" and $1a_2'$ are pure ligand MO's. The four lowest Al_3^+ valence MO's ($1a_1'$, 1e' and $1a_2''$) are O–Al bonding. The next two MO's ($2a_1'$ and 2e') are antibonding in this respect, but have Al–Al bonding character. On this basis, Al_3O^+ can be said to prefer the D_{3h} structure, because the 2e'-HOMO is fully occupied by four electrons and the HOMO–LUMO energy gap is very large. If the unpaired electron in the neutral Al_3O molecule occupies the 3e'-MO, C_{2v} distortion to Y- or T-type structures occurs (see Figure 1). Relative to the D_{3h} geometry, these distortions result in increased Al–Al bonding. If

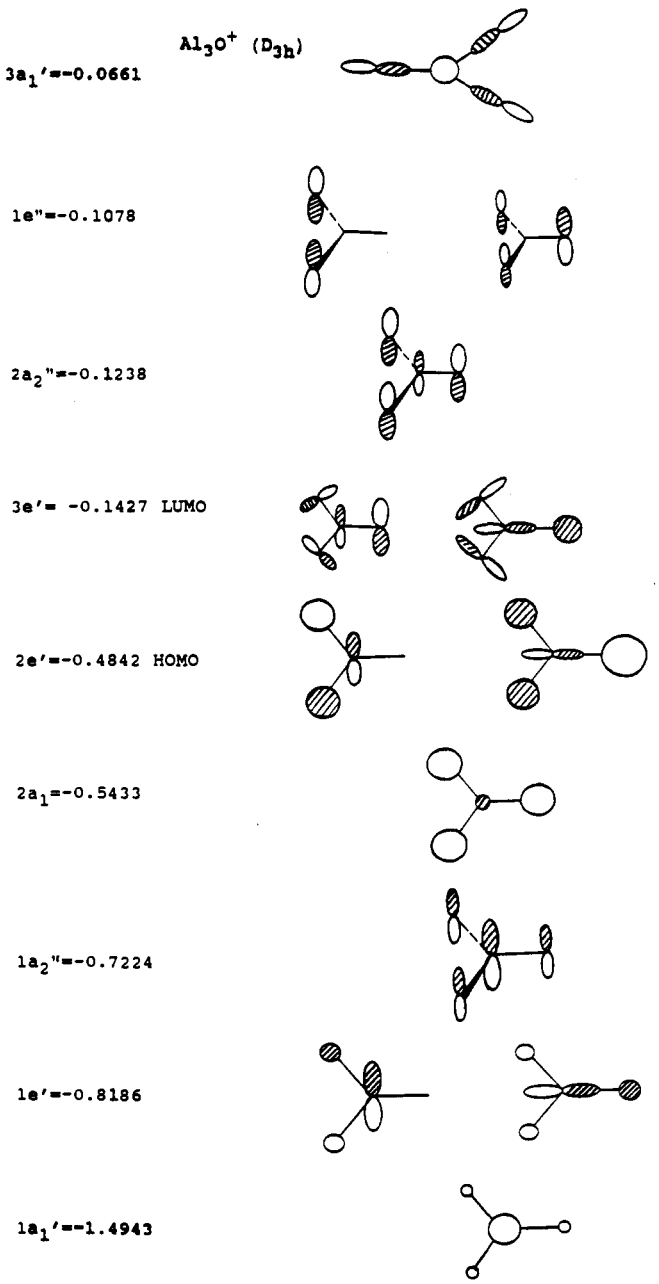

Figure 6. MO scheme of Al_3O^+ (D_{3h}).

the unpaired electron occupies the $2a_2''$-MO, a C_{3v} structure is found, but this minimum is higher in energy than the C_{2v} forms because of the less effective overlap.

The qualitative MO scheme for Al_3O^+ also provides insights in comparison with Li_3O^+. The first eight valence electrons of both fill the $1a_1'$-, 1e'-, and $1a_2''$-MO's which are central atom–ligand bonding. The next MO's ($2a_1'$, 2e', 3e', $2a_2''$, and 1e") have antibonding or nonbonding central atom–ligand character, but are ligand–ligand bonding. Hence, molecules in which such MO's are occupied may be stabilized by ligand–ligand interactions. Neutral Li_3O and Al_3O are examples. In Li_3O, the ninth valence electron occupies the $2a_1'$-MO, but in Al_3O five "extra" valence electrons are available for the $2a_1'$-, 2e'-, and 3e'-MO's. A further increase in the number of valence electrons would lead to greater antibonding central atom–ligand character. After a certain limit in the number of electrons is reached, structures with the oxygen atom outside the M_3 or M_4 moieties should be more stable than structures (like Li_3O, Al_3O, Li_4O, and Al_4O) with oxygen inside. (For example, P_4O might be expected to have oxygen outside the P_4 cluster.) An investigation along these lines is in progress. Similar qualitative considerations apply to other cases with heteroatoms other than oxygen, and these are being studied as well.

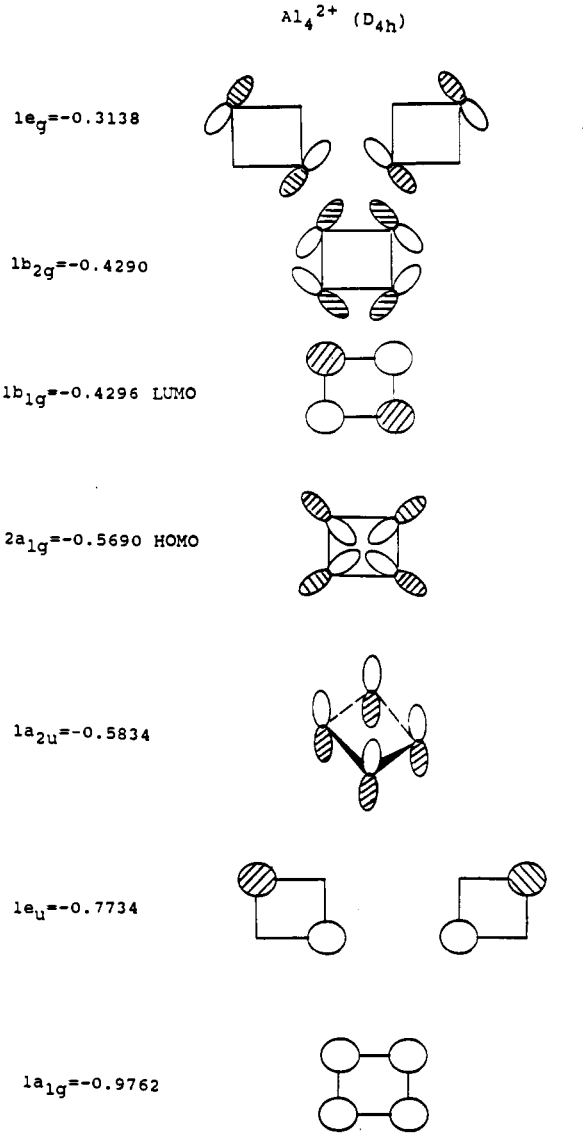

Figure 7. MO scheme of Al_4^{2+} (D_{4h}).

The qualitative MO schemes for D_{4h} symmetry, involving Al_4^{2+} and Al_4O, are given on Figures 7 and 8. Again, the MO's of Al_4O may be derived from the MO's of Al_4^{2+} and the AO's of O^{2-}: $1a_{1g}$-MO ($1a_{1g}(Al_4^{2+}) + 2s(O^{2-})$), $1e_u$-MO ($1e_u(Al_4^{2+}) + 2p_x,2p_y(O^{2-})$), $1a_{2u}$-Mo ($1a_{2u}(Al_4^{2+}) + 2p_z(O^{2-})$), $2a_{1g}$-MO ($1a_{1g}(Al_4^{2+}) - 2s(O^{2-})$), $2e_u$-MO ($2p_x,2p_y(O^{2-}) - 1e_u(Al_4^{2+}) + 2e_u(Al_4^{2+})$), $1b_{1g}$-MO (pure $1b_{1g}(Al_4^{2+})$), $1b_{2g}$-HOMO (pure $1b_{2g}(Al_4^{2+})$), and $2a_{2u}$-LUMO ($1a_{2u}(Al_4^{2+})$-$2p_z(O^{2-})$). The first valence $1a_{1g}$-, $1e_u$-, and $1a_{2u}$-MO's are central atom–ligand bonding and either bonding or nonbonding with respect to ligand–ligand interactions. In Li_4O, only these five valence MO's are occupied; hence, this molecule is stable toward dissociation. In Li_4O and in Al_4O these MO's are comprised primarily of the 2s- and 2p-AO's of O^{2-}. This dianion is stabilized by the field of Li_4^{2+} or Al_4^{2+} dication cage. In Al_4O (D_{4h}) the next higher valence $2a_{1g}$-, $2e_u$-, $1b_{1g}$-, and $1b_{2g}$-MO's are fully occupied. All these MO's are mainly ligand AO's; only the $1b_{1g}$-MO is ligand–ligand antibonding. Hence, bonding Al–Al interactions contribute to the stability of Al_4O. Because the LUMO of Al_4O as well as higher unoccupied MO's (up to $3a_{1g}$) also have predominate ligand–ligand bonding character, similar to M_4O molecules with electropositive ligands M and a greater number of valence electrons may also be stable toward dissociation. But, as discussed above, increasing the number of valence electrons will lead eventually to an increase in the antibonding central atom–ligand interactions. Alternative structures with the oxygen dianion outside of the M_4 moiety will be favored increasingly. An example already is provided by the C_{3v},I triplet form of Al_4O, in which the O^{2-} dianion lies outside

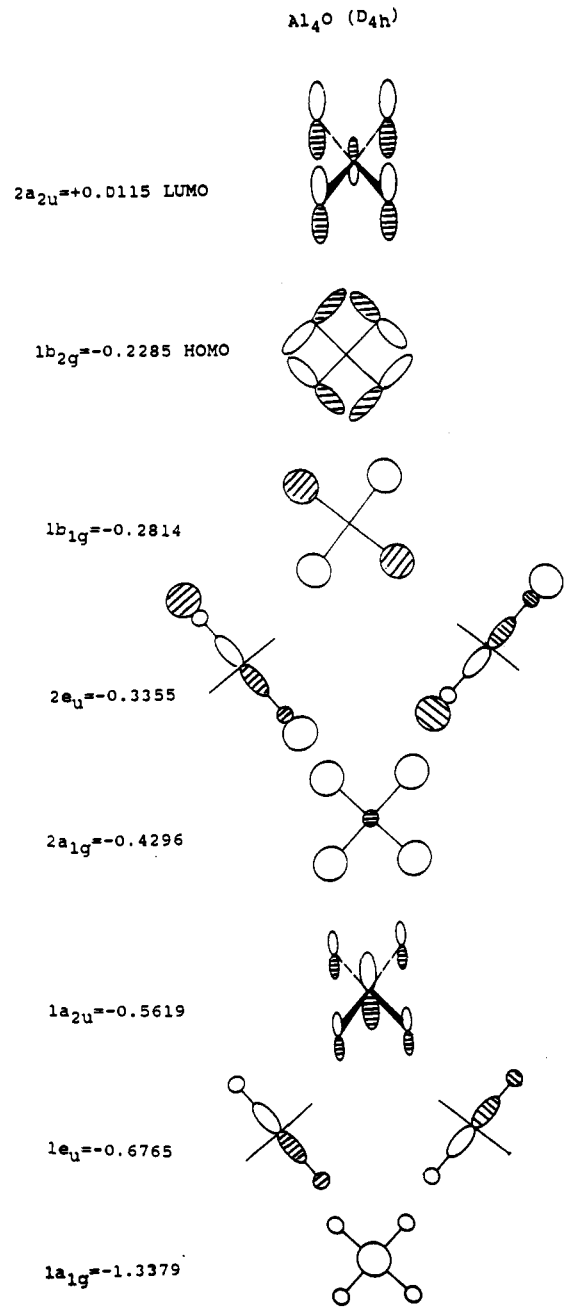

Figure 8. MO scheme of Al_4O (D_{4h}).

the Al_4^{2+} cage. This structure is only a few kcal/mol higher in energy than the singlet D_{4h} global minimum at HF/6-31G*, but correlation increases this difference substantially.

Other species which employ ligand–ligand interactions effectively may be also stable. The Al–Al distances in C_{2v},I and C_{2v},II structures of Al_4O ($^1A_1$) are quite short. These singlets lie above the D_{4h} form by 1.4 and 9.1 kcal/mol at HF/6-31G*, respectively. Likewise, the triplet C_{2v},I is the most stable structure of Al_4O at HF/6-31G*. But correlation energy favors the singlet planar square D_{4h} form preferentially. This also shows the importance of covalent, multicenter bonding in Al_4O. Wholly ionic species have localized character; their relative energies typically are little influenced by correlation corrections.

Finally, it is interesting to consider the stability relationship of the aluminum oxides along the AlO–Al_2O–Al_3O–Al_4O series (Table I). The first two members have very high dissociation energies (e.g., well over 100 kcal/mol for loss of an Al atom) because of the highly ionic bonding Al^+O^- and $Al^+O^{2-}Al^+$. As the maximum oxygen charge is 2– (note Figure 3; oxygen has nearly the same effective charge in Al_2O, Al_3O, and Al_4O), the total electrostatic Al–O bonding does not improve when more Al ligands are present. However, the ligand–ligand bonding does increase. Indeed, the energies of dissociation of Al_3O into AlO + Al (19.9 kcal/mol) and Al_4O into Al_3O + Al (45.5 kcal/mol) or into Al_2O + Al_2 (37.1 kcal/mol; all at PMP4SDTQ/6-311+G* + ZPE) are similar to $D_0(Al_2)$ = 35.7 ± 1.0 kcal/mol[48] (see Table I). (For Al_3O, the dissociation into AlO and Al_2 is less favorable for the combination of reasons discussed above.)

Conclusions

The main conclusions of this study are the following.

(1) The hyperaluminum Al_3O and Al_4O molecules are stable with respect to all possible modes of dissociation. Al_3O prefers planar triangular Y- and T-type geometries (these have nearly the same energy and this molecule is highly flexible with respect to in-planar intramolecular rearrangement). Al_4O adopts a square-planar singlet structure. The calculated frequencies for these species may help their identification in matrix isolation experiments. Several additional Al_3O and Al_4O minima in both singlet and triplet states were identified, but these are significantly higher in energy at electron correlated levels.

(2) Although we predict Al_3O to have a substantially lower dissociation energy than Al_4O (e.g., 19.9 versus 45.5 kcal/mol, respectively, for loss of an Al atom), there only is mass spectrometric evidence for the former as yet.[20] A deliberate search for Al_4O experimentally should be successful.

(3) The high degree of ionic character as well as bonding interactions between the aluminum atoms is responsible for the stability of these hypermetalated species. Al–Al interactions are largely responsible for the greater stability of Al_4O over Al_3O.

(4) These findings should be general. Other hypervalent M_nX molecules, where n is higher than the normal valence of the central atom X and M is an electropositive ligand (other than alkali or aluminum), are likely to be stable because of the combination of electrostatic and bonding ligand–ligand interactions.

Acknowledgment. This work was facilitated by an Alexander-von-Humboldt Fellowship to A.I.B. and was supported by the Fonds Der Chemischen Industrie, the Stiftung Volkwagenwerk, the Deutsche Forschungsgemeinschaft, and the Convex Computer Corporation.

Registry No. Al_3O^+, 136060-69-0; Al_3O, 136060-68-9; Al_4^{2+}, 136060-67-8; Al_4O, 136060-66-7.

Supplementary Material Available: Tables of total energies of different forms of aluminum oxide species at UHF/6-31G* (Table 1S) and at different correlated levels (Table 2S) (4 pages). Ordering information is given on any current masthead page.